**Structural analysis of Heinz Isler's bubble shell**

P. Eigenraam*, Delft University of Technology, P.Eigenraam@tudelft.nl, Julianalaan 134, 2628BL, Delft, The Netherlands

A. Borgart, Delft University of Technology

J. Chilton, University of Nottingham

Q. Li, Nanjing University

*Corresponding author

**Abstract**

This paper presents a detailed structural analysis of a bubble shell engineered by Heinz Isler. Through 3D scanning the geometry of this shell structure has become available to the authors. Structural analysis has not been possible before since the geometry of the shell was not available. The bubble shell was Isler's most built type of shell. In the paper first the process of reverse engineering the geometry of the shell is described. Second, the effect of pre-stress in the edge beams is described. Third, the load distribution throughout the shell and the membrane behaviour relative to bending behaviour is assessed.

**Keywords**

Heinz Isler, shell structures, structural analysis, physical models, reverse engineering, finite element analysis, pre-stress, shell behaviour

**Introduction**

The results of the work of Heinz Isler (1926-2009) are very well known among engineers and architects. He has engineered numerous shell structures, mainly in his home country Switzerland. Among other types, the bubble shell is Isler's most built type of shell. Detailed structural analysis by others than by Isler himself has, until now, not been possible. From Isler's archive only two cases have been found where Isler provided geometry. Namely, to Prof. D. P. Billington of Princeton University (late 80's) [1] and Prof. F. Frey of the École Polytechnique Fédérale De Lausanne (1993) [2]. But these were not meant to be publically available. Also, one of the authors has knowledge of Isler providing geometry to Prof. E. Ramm. Now, through 3D scanning (July 2011) and reverse engineering of Isler's models the geometry has become available to the authors [3]. This paper presents for the first time a detailed structural analysis of a bubble shell. In Figure 1 a photo of Heinz Isler on top of his bubble shells can be seen close to his office in Lyssachschachen in 2006.

When Heinz Isler died in 2009, he left a large collection of models and documentation which was not publically available until then. The models and documentation was bequeathed to the Institut für Geschichte und Theorie der Architektur (GTA), Eidgenössische Technische Hochschule (ETH) in Zurich. At the moment of writing, the collection is in process of being archived. The analyses in this paper are supported by information found in this archive.

*Figure 1 Heinz Isler on the roof of bubble shells in Lyssachschachen in 2006 (Photo: ©wilfried-dechau.de)*

An elaborate description of the bubble shells is given by E. Ramm [4] and J. Chilton [5]. Most of the shells were for industrial purposes. Therefore, apart from "bubble shell" the shells are sometimes referred to "industrial shells" in both English and equivalent in German language. Isler himself has described the advantages of the bubble shells [6]. Here, he mentions for example the large free space and openings in the façade and that the shell is without cracks, so is therefore waterproof. In general demands from authorities for lighting, sound reduction, fire protection, fast drainage and durability are easily met. Also, the shells can harmonize better than traditional industrial buildings in the vicinity of non-conventional buildings. The shells have edge beams along the perimeter in which pre-stressed, post-tensioned, tendons are integrated. The shell is lifted from the ground with columns placed at the corners. The shape of the bubble shell was created using an inflated membrane model. This method was inspired by a plumped-up pillow which Isler observed in 1954 and led him to a solution for a shell structure on a rectangular plan which he was working at that time. Since then the bubble shell has developed. Bubble shells were designed and built in various sizes between 15 and 58.8 m span with square or rectangular plans. Most are applied in clusters of multiple connected shells. Within the plan of these buildings the columns would be at relatively large distance from each other, thereby creating well-conceived, functional and flexible spaces suitable for industrial purposes.

There are two aspects in particular that Isler mentions which are of interest for this paper: first, *"By means of an appropriate pre-stress, and applying the science of modern concrete technology, the whole shell is, and remains, waterproof"* [6]. Second, the transfer of load within the shell mainly is directed towards the corners [5]. Both these aspects will be elaborated.

Isler determined the structural behaviour of his shells by means of physical models, using techniques that he learnt whilst working as an assistant in the laboratory established by his mentor Professor Pierre Lardy (1903-1958), at ETH, in the early 1950s. Figure 2 shows a Plexiglas model of a bubble shell, where Isler was able to apply alternative loading configurations, including pre-stress of the edge beams, and measure resulting effects such as vertical displacements, strain and pre-stress force [7]. Although the authors have searched on several occasions specifically for analytical attempts by Isler to describe the structural behaviour of the bubble shell, none have been found in the Isler archive until the time of writing (August 2019).

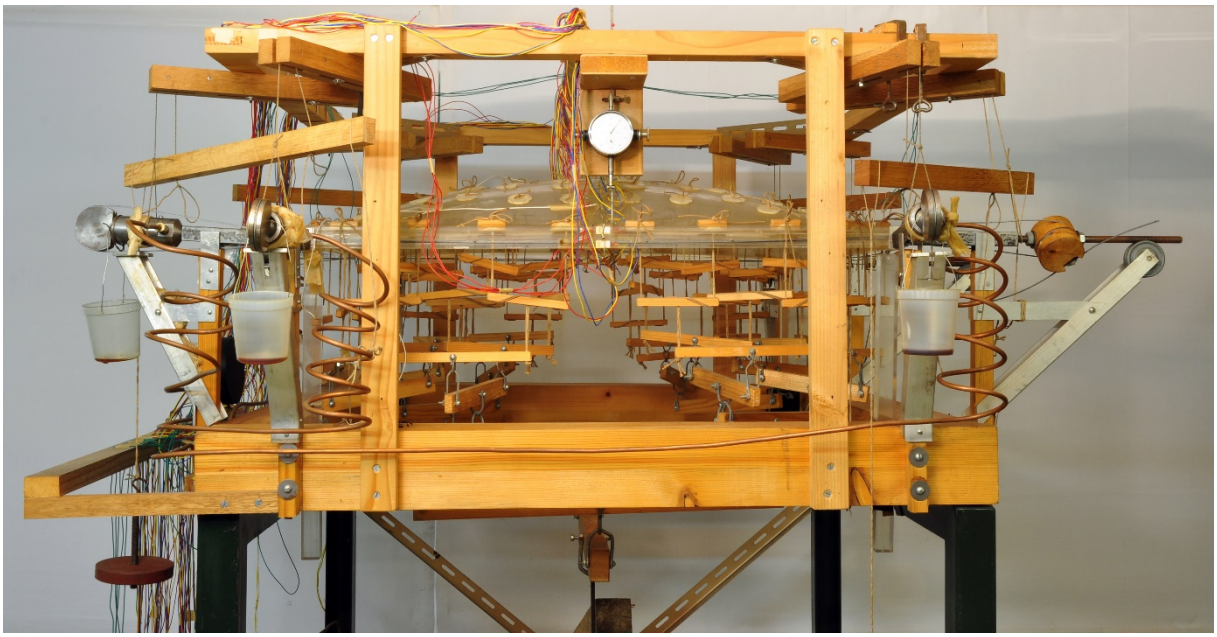

*Figure 2 Measuring model of Heinz Isler (Photo: © gta Archives / ETH Zurich, Heinz Isler Archive - 217)*

Isler's methods of engineering are known in a general manner. He describes these himself in various publications and he has taught them to students. An overview of Isler's publications until 2002 has been provided by Ramm [4]. However, typically the level of detail in the descriptions and drawings remains limited. This was found through reverse engineering of Isler's work in which all steps had to be traced. Isler himself makes related comments on this in the context of education in a personal letter to D.P. Billington. He distinguishes four consecutive levels of teaching of which the last two he has never taught [1]. Isler ends the letter by comparing shell design to painting; "no one would start a lesson by letting (students) copy Rembrandt".

This paper describes how the geometry of a bubble shell was obtained and processed into a finite element analysis (FEA) model. Further, the results of the FEA are presented. Three aspects are investigated in particular: first, the general structural behaviour of the shell under self-weight only; second, the effect of pre-stress on the structural behaviour; and lastly, membrane behaviour is studied comparing ratios of stress induced by bending and normal forces.

**Geometry of the shell**

The geometry of this model is derived from a physical model in Isler's former office in Lyssachschachen. The scale model has been scanned as described in [3]. This method makes use of a 3D scanner and results in a point cloud. The scan is shown in Figure 3 where two models of the bubble shell can be seen (top left and bottom centre). The physical model has a size of 40 x 40 cm. This would be a 1:50 scale model for a 20 x 20 m shell which is one of the standard sizes constructed by Isler. The point cloud has been scaled to this size for further modelling.

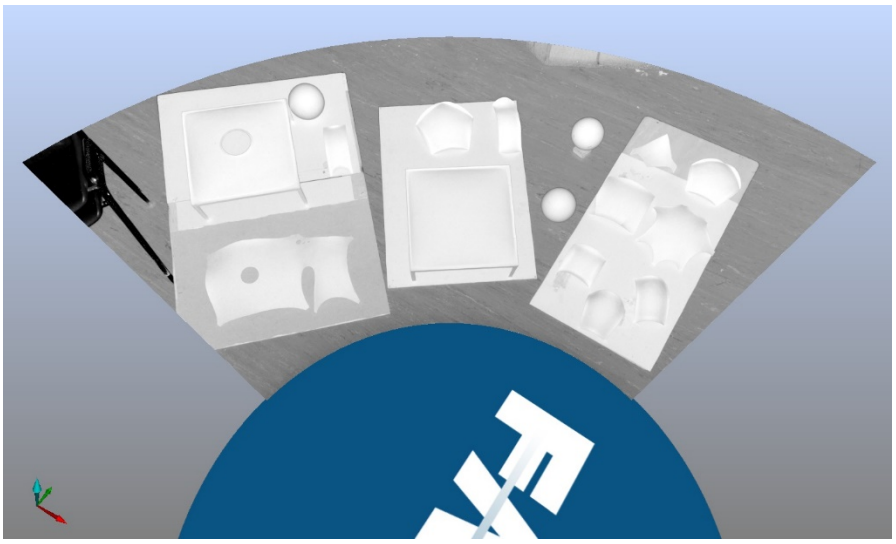

*Figure 3 Visualization of 3D scan of a number of models with two bubble shells (top left and bottom centre)*

A Non-Uniform Rational B-Spline Surface (NURBS) has been fitted to the point cloud according to a method described in [3]. Initially various surfaces were fitted in order to find a best fit. These had different grid densities of control points and have been compared for accuracy of fit. The degree of the used NURBS surfaces is 5 such that a high level of geometric continuity is secured. Figure 4 shows the point cloud and a fitted NURBS surface. Modelling was done in the 3D modelling software Rhinoceros [8]. Figure 5 shows the statistical data of accuracy of fit for each surface on the point cloud. It can be observed that after increasing the grid density to 8 x 8 no significant improvement in accuracy was achieved. But smoothness may decrease with a denser grid. Therefore an 8 x 8 grid was used for further modelling.

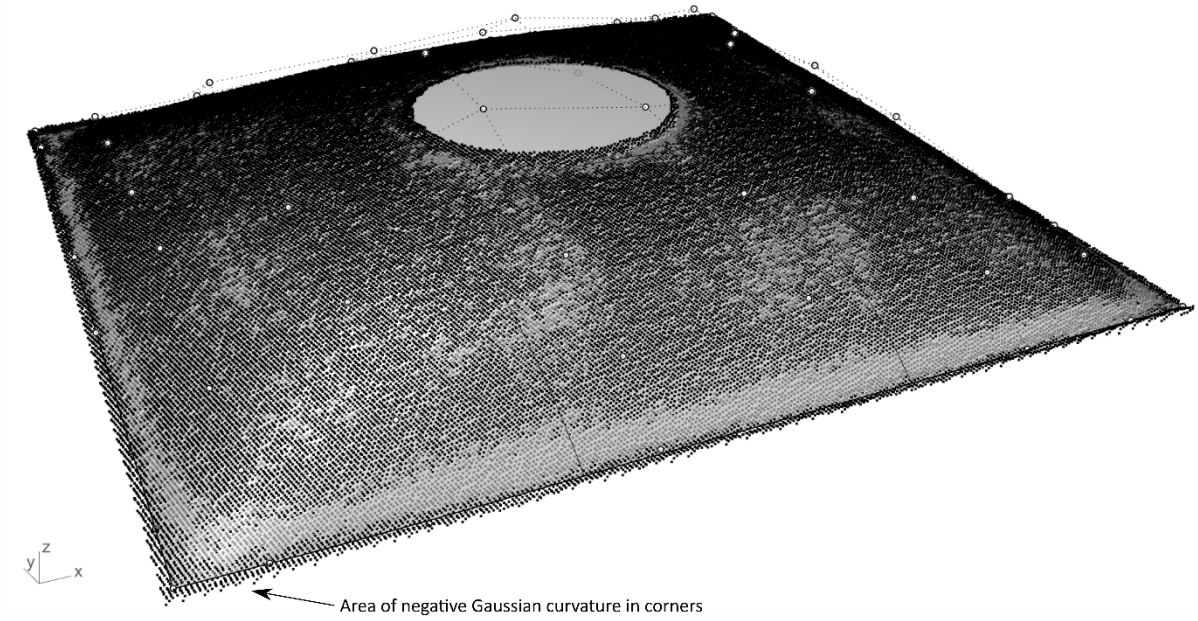


*Figure 4 Point cloud (black) and a fitted NURBS surface (grey) with an 8 x 8 grid of control points (white)*

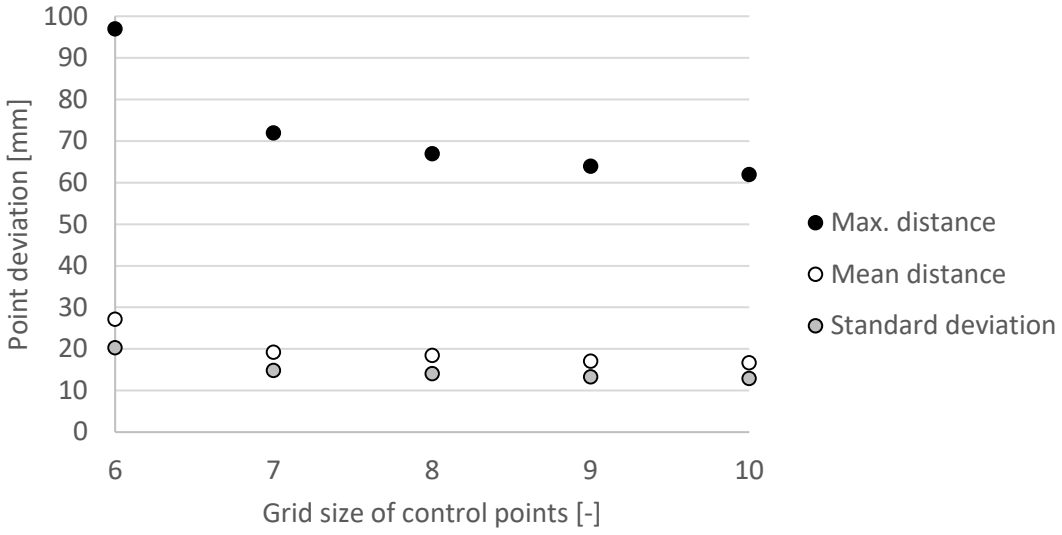


*Figure 5 Statistical data of accuracy of fit for various NURBS surfaces*

Isler found that inflating a membrane bounded by a rectangular boundary results in negative Gaussian curvature in the corners. Applying vertical load to anticlastic surfaces results in tensile forces. Isler wanted to avoid these and changed the rectangular boundary by rounding off the corners. Thereby the entire shape of the inflated has positive Gaussian curvature. The complete structure extends to a rectangular plan. However, the actual shell does not extend to the perimeter of the structure. It starts at the inner face of the edge beam, as can be seen in Figure 16.~~The distance between the edge of the shell and the perimeter of the structure is edge beam.~~ These two parts of the structure must be considered separately. For the shell surface the scanned geometry of the edge beam has been excluded by taking into account a smaller rectangle of 19.5 x 19.5 m according to the actual geometry of the shell. This does not fully remove the horizontal surfaces in the corners and the fitted surface remains synclastic in that area. A manual modelling approach was adopted to correct the corners taking into account the tangencies of the adjacent shell surfaces. The finally obtained surface ~~model~~ can be seen in Figure 6.

The point cloud showed slight asymmetry. This has been averaged such that a symmetric model has been obtained. The opening in the centre has been left out to simplify the model.

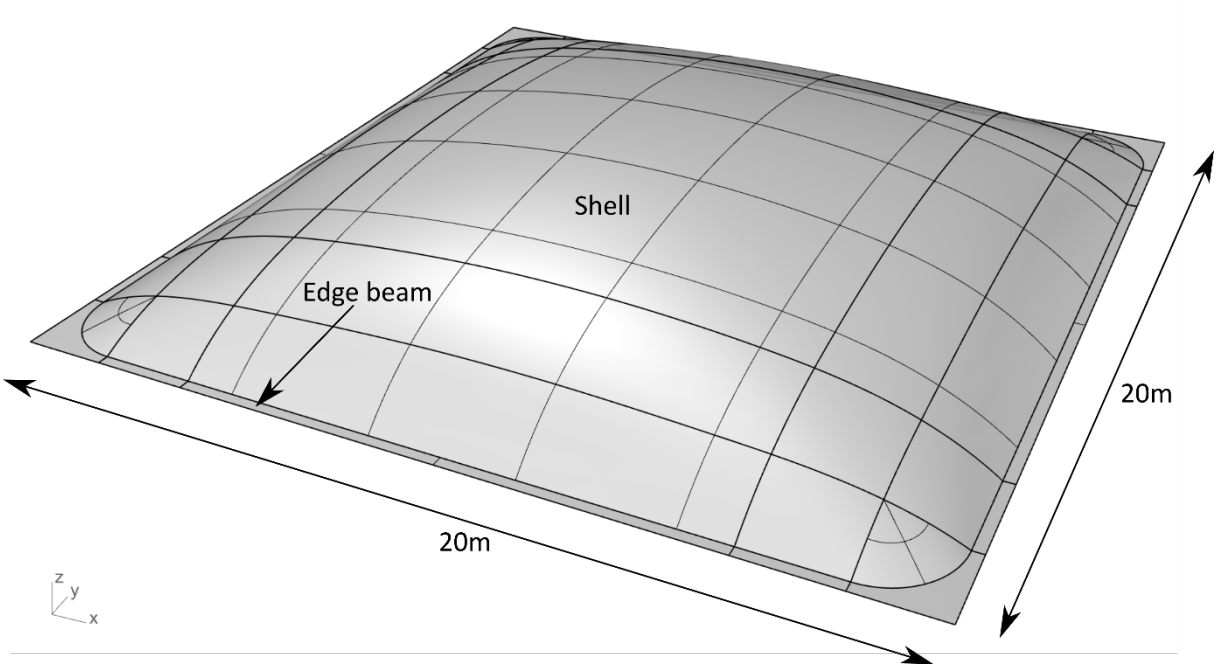


*Figure 6 Surface model after reverse engineering of the point cloud*

In the broader context of this research the authors have reverse engineered several of Isler's shells. The process has shown that reverse engineering of shell structures cannot be defined as an identical sequence of steps every time. Each shell presents specific challenges. In the model of the bubble shell three aspects required special attention: (1) obtaining the geometry of the shell without edge beams, (2) modelling of the rounded corners and (3) modelling of the edge beams.

**Reverse engineering of the shell surface**

Detailed steps for the reverse engineering of the shell surface will now be described. The basic method of reverse engineering has been described for a relatively simple shape in [3]. The location of the control points has been determined as follows: (1) a planar 8 x 8 grid was aligned with the base of the shell; (2) a temporary NURBS surface with 19 x 19 grid was fitted to the point cloud; (3) all grid points were projected onto the NURBS surface in a vertical direction; (4) these projected points were then averaged with those that corresponded to their equivalent points with respect to symmetry of the shell; (5) a surface was created that intersects these points. Therefore, the positions of the control points differ from the obtained points. Control points define NURBS surface but do not lie on the surface. The positions have been obtained by a common function within the software package Rhinoceros [8] and Grasshopper [9] called "Surface from points" [10].

To obtain the rounded corners of the shell, surfaces have been modelled such that the corner surface follows the rounded edge and is tangent to the shell surface. This way the typical rounded edge corners prevent Gaussian curvature reversal. The edge beams around the shell were modelled as planar surfaces and match the outside perimeter of 20 x 20 m.

Dimensions of the shell, edge beams and columns are based on drawings by Isler [11] which are present in the GTA Archive in Zurich. The drawing is shown in Figure 7. The archive contains drawings for many shells and different dimensions of the beams. Each specific context seems to require different dimensions, for instance, when the edge beams facilitate overhead cranes. The chosen shell is 20 x 20 m in plan without overhead crane. Some of dimensions were not given, then an estimation has been made based on text and figures from Ramm [4] and Chilton [5]. The general overall thickness of the

shell was chosen to be 80 mm. All Isler's drawings show a varying thickness tapering from the edges towards to centre of the shell. This was implemented for the present analysis in a co-linear manner, namely, 160 mm at the edge beam linearly decreasing to 80 mm over 500 mm in the positive z-direction (upward) from its base. Edge beams coincide with the edge of the shell. The beam height and width were chosen to be 550 x 250 mm, ignoring the upstand forming the gutter. Due to the width of the beams the shell area has been modelled with a width of 19.5 m. This way the model including the width of the beams is 20 x 20 m overall. Columns have been chosen to be 600 x 600 mm and a length of 7.5 m.

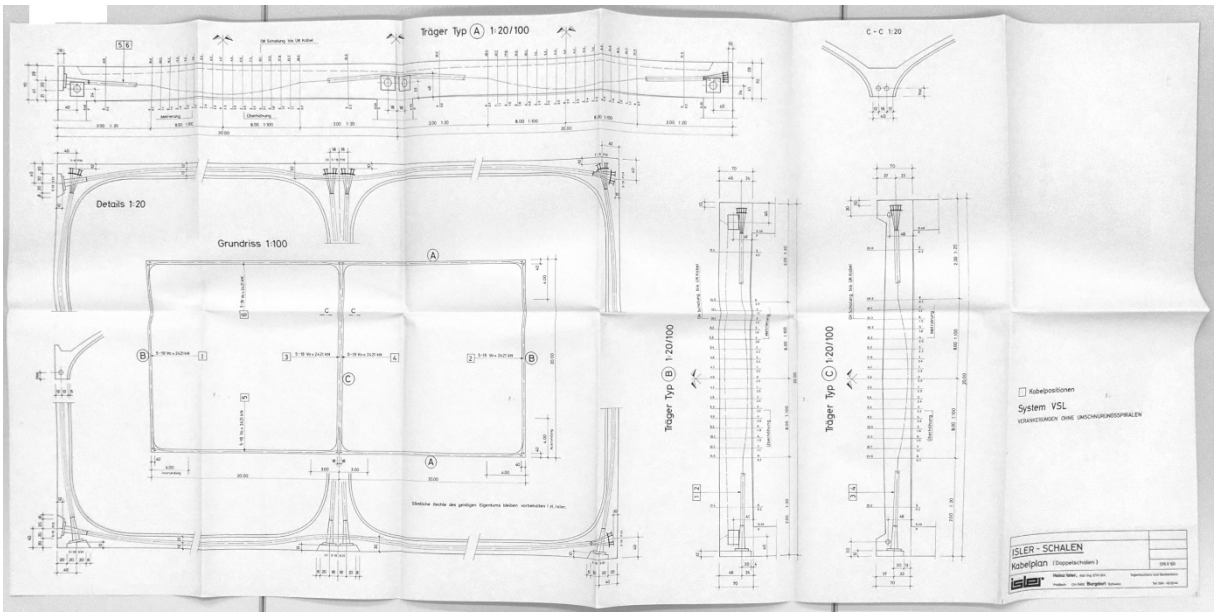


*Figure 7 'Kabelplan' drawing of a 20 x 20 bubble shell by Isler (Photo: G. Boller taken from © gta Archives / ETH Zurich, Heinz Isler Archive - 217)*

**Finite element model**

The finite element model has been made within the software package DianaFEA [12]. Isoparametric degenerated solid elements (2.5D) have been used for the shell and the edge beams. These are Mindlin-Reissner elements. It's polynomial function for translations *u* are similar to the implicit interpolation of a serendipity eight-node rectangle plane stress element. The elements have eight nodes per element and 5 degrees of freedom per node. At the connection of the shell and edge beams all degrees of freedom are connected (by default). The details in Figure 7 show that the shell and edge beams are a monolithic structure. The shell and the edge beams have been given different thickness according above described dimensions. The columns have been modelled with beam elements. These are curved higher order elements with three nodes per element and 6 degrees of freedom per node. At the connection of the column and edge beams dummy elements have been added in a grid pattern. Thereby the problems arising from singularities at the connecting node have been resolved. The forces are distributed over multiple elements and local distortions are avoided. The dummy elements have been given the same cross section as the columns and Young's modulus of concrete, but zero weight. The mesh types used are respectively CQ40S and CL18B of which the details can be found in the Diana FEA manual [13]. The mesh can be seen in Figure 8, where the dummy elements at the column/edge connections are shown in red.

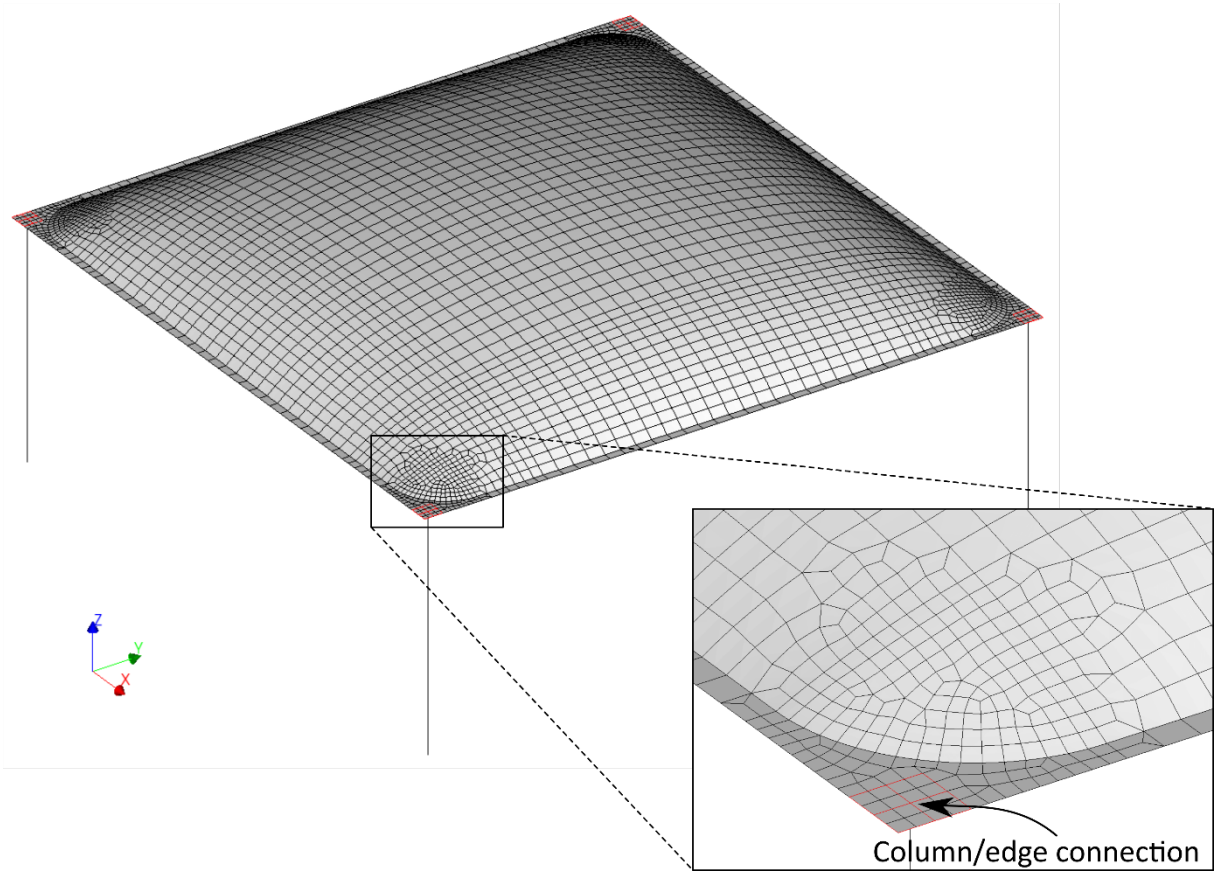


*Figure 8 Outside view of finite element mesh*

The supports, at the bottom of the columns, are assumed to be fully constrained. In analytical calculations Isler used these conditions for wind load analysis. An example of that has been found in his archive. Therefore, in the FEA model all degrees of freedom are constrained (Tx, Ty, Tz, and Rx, Ry, Rz).

The Young's modulus of concrete was chosen as 20000 N/mm$^2$. Therefore, it is assumed that the concrete remains un-cracked. The specific weight was chosen to be 2500 kg/m$^3$.

Two loads have been applied in three load cases, namely: LC1 self-weight, LC2 pre-stress, LC3 self-weight + pre-stress. Since the thickness of the shell varies, the self-weight load was determined automatically by the FEA software. Pre-stress was applied by equivalent external loading which was determined in a manner applied by Isler himself. This was found in his archive and shown in Figure 10 [14].

The shape of the pre-stressed tendons is assumed to be parabolic. By its curvature it creates an upward distributed load and axial forces in the direction of the tendons. In vertical planes, bending moments by eccentricity to the centroid at the ends of the beams are neglected. These bending moments are small compared to the maximum bending moment due to the upward load. In the bottom left corner of Figure 7it can be seen that the tendons start eccentric to the centreline of the edge beams. The resulting bending moments are in equilibrium. Therefore, these do not apply additional loading. The distributed load was determined from the geometry and equilibrium of forces as shown in Figure 9 and equations (Eq. 1) and (Eq. 2):

$$\frac{2f}{\frac{L}{2}} = \frac{V}{H} \quad (1)$$

$$q = \frac{2V}{L} \quad (2)$$

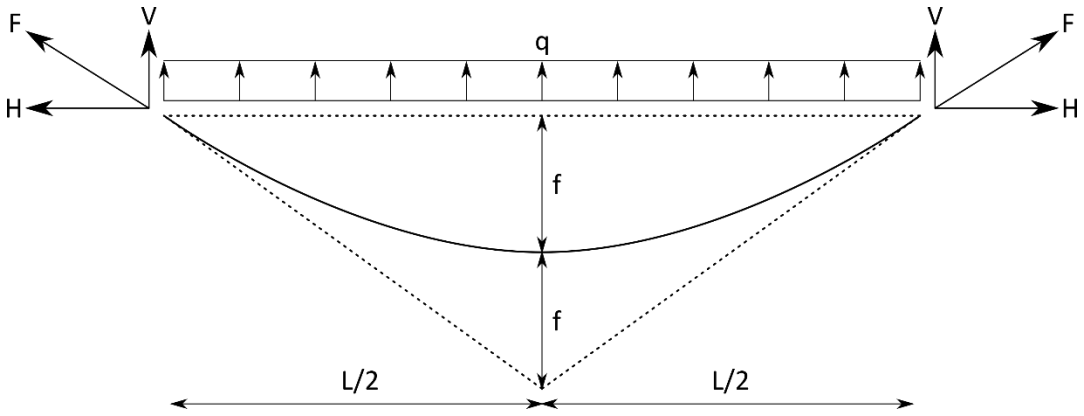


*Figure 9 Equilibrium of a pre-stress tendon*

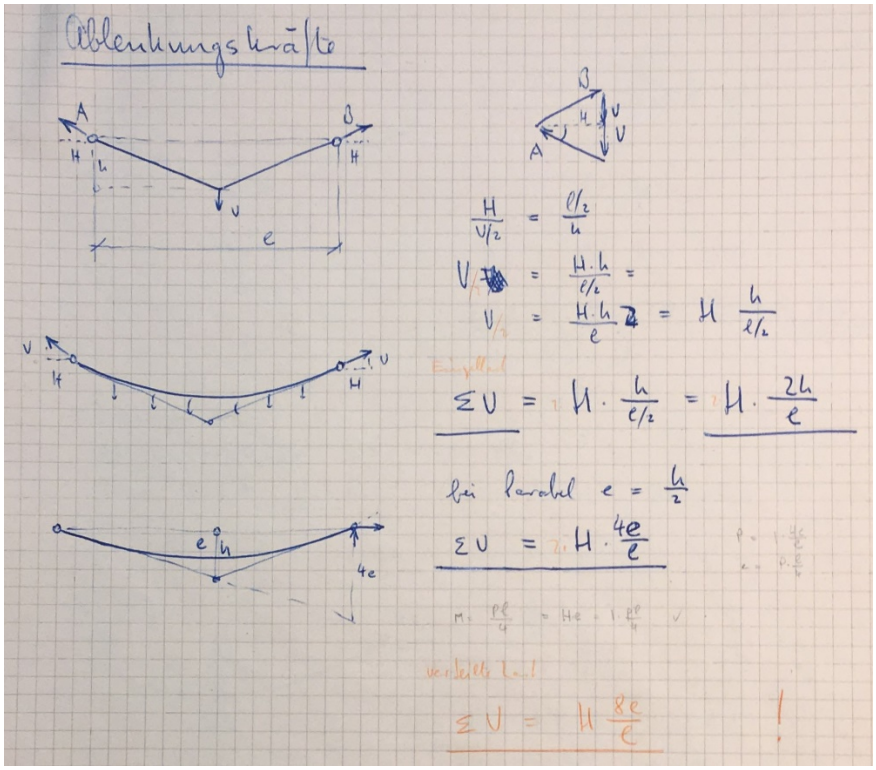


*Figure 10 Derivation of forces in a pre-tensioned cable by H. Isler (Photo: Eigenraam taken from © gta Archives / ETH Zurich, Heinz Isler Archive - 217)*

From Isler's drawings it is found that the height of the parabola (f) varies for different edge beams, namely, 20, 29 and 37 cm. A typical free edge beam, which is identical to this model, has the height of 20 cm. Therefore, this height is used for f and the length (L) is 20 m.

The applied pre-stress force (H) is 2421 kN according to the drawing. However, it is generally known that the effect of pre-stress becomes less due to a number of factors, for example: anchor seating, elastic shortening of the concrete, friction of the tendon and tube, concrete shrinkage, creep, and tendon relaxation. This is known as pre-stress losses [15]. Precise calculation of these losses would require information that was not available. Therefore, the losses are assumed to be 20%, which is a typical value for this application. The effective pre-stress force is therefore chosen to be 1937 kN. Using Eq. 1 and 2, this results in an equally distributed load (q1) upward of 7.748 N/mm. This was applied as a surface load to the edge surface which has a width of 250 mm width. The load therefore is 0.030992 N/mm$^2$.

In the horizontal plane, at the start and end, the tendons curve over a distance of 4 m resulting in a horizontal distributed load over this length. Similar to the above this load is determined as follows. From the drawings it has been derived that f is approximately 70 mm, the effective pre-stress force is equal to 1937 kN and the length L is 4 m. This results in an equally distributed load (q2) of 67.795 N/mm. This load could be applied as a line load. These loads together are represented in the scheme of Figure 11.

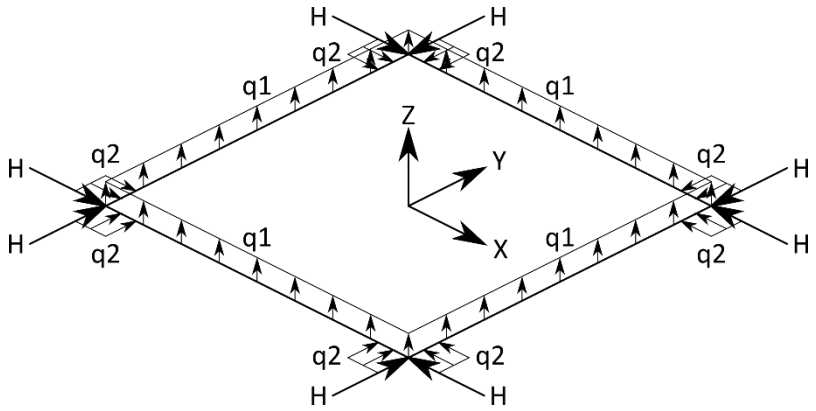


*Figure 11 Pre-stress load diagram at the perimeter of the bubble shell*

The geometry represents the upper surface of the shell. However, in finite element modelling the geometry represents the middle surface of the shell. Therefore, in the FEA model, an offset of half the thickness was applied downward for the entire shell. In this way the top surface of the shell elements aligns with the point cloud and modelled geometry. This is shown in Figure 12 for the corner of the shell. The red curve shows how the geometry corresponds to the mesh. The edge beam has been given an downward offset , so that the centroid is 180 mm lower than the surface to match the drawing as close as possible.

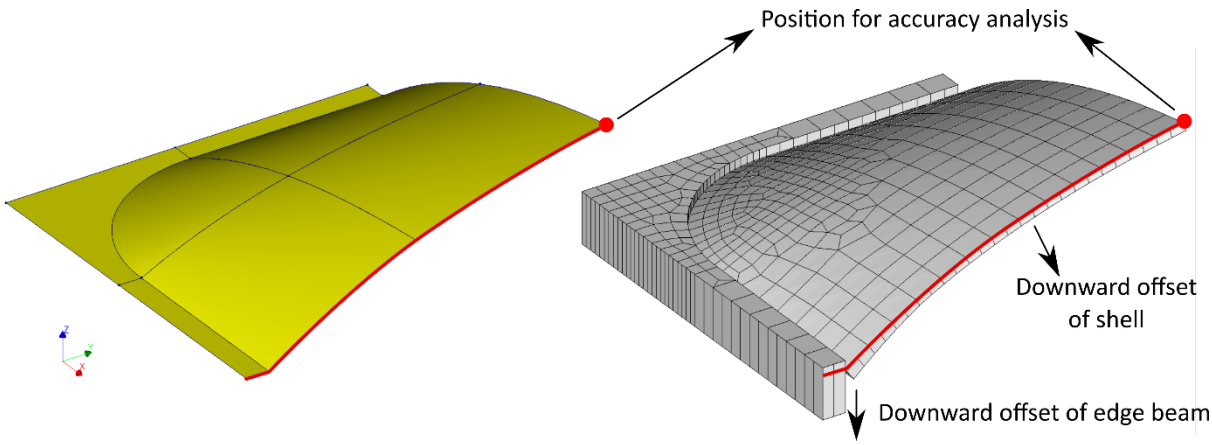

*Figure 12 Shell corner geometry (left) and mesh displayed with set thickness and eccentricities (right)*

Accuracy analysis was done in order to select the mesh size. Difference meshes using a mesh size of 1000, 500 and 250 mm were compared. The analysis was done by estimating the numerical mathematical error present as the result of truncation of the polynomial functions, which is inherent to any finite element analysis. This method has for example been described by ~~using a method described~~ by Zienkiewicz et al. [16] and Kok [17]. The analysis has been made using the stress in local x-direction of the bottom layer and deflection in z-direction due to self-weight only. The position for the analysis is indicated in Figure 12. At the corners a mesh size of 150 mm was chosen, thereby creating a smooth transition to the dummy elements at the corners. In the analysis *n* is the relative division, *h* is the relative error and $r_e$ is the improved estimation of the result based on two models. The shell elements used possess an accuracy of $O(h^2)$ according their interpolation polynomials. Based on the analysis a typical mesh size of 500 mm was chosen.

| Mesh size [mm] | 1000 | | 500 | | 250 |
|---|---|---|---|---|---|
| n | 1 | | 2 | | 4 |
| h | 1 | | 0,25 | | 0,0625 |
| | | | | | |
| Sxx | -1,237 | | -1,241 | | -1,245 |
| $r_e$ | | -1,242 | | -1,246 | |
| Error | **0,41%** | | **0,42%** | | |
| | | | | | |
| DtZ | -6,062 | | -6,040 | | -6,042 |
| $r_e$ | | -6,033 | | -6,042 | |
| Error | **0,48%** | | **0,02%** | | |

*Table 1 Accuracy analysis for various mesh size*

A last comment on the FEA model also applies for shell analysis in general and requires some additional steps of thought before coming to a conclusion. Ideally a shell would have no bending moments resulting in zero bending stress. When considering compression only structures there is some margin for bending moments until the by bending induced tensile stress exceeds the compression caused by normal force. This margin however is not very large. Stresses caused by the normal force are distributed through the entire cross section. Therefore, they usually remain small. Bending moments easily result in the same stress on an outer surface. A bending moment can be considered as an eccentric applied force with respect to the centroid. When the eccentricity of the force is equal to 1/6 of the thickness, the stress due to bending and normal force is equal~~n eccentricity of only 1/6 of the shell thickness is sufficient for equal stress due to normal force and bending as total stress due~~, as shown in Figure 13. This is also known as the middle third rule. This leads to two problems, especially for thin structures.

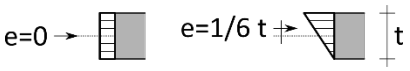


*Figure 13 Stresses according to middle third rule*

The first is worth mentioning, although no practical means are available for implementation in these models. The thickness of Isler's shells roughly varies between 80 and 100 mm. Now, assuming a perfect compression surface was found, it must also be built with a tolerance of approximately 1/6 of the thickness which is 13-16 mm. This, even for today's standards, is very hard to achieve, especially for large span structures.

A second problem is the following: even when the perfect shape can be built perfectly, in-plane forces cause in-plane strain since the material is considered elastic. This results in deflections which cause

eccentricity of the load. When a significant part of the load is distributed through in-plane force the results may be influenced when deflections are close to or exceed 1/6 of the shell thickness. This deflection is easily reached. It should be noted that, in general, the effect will relatively be less in parts of the shell which are already in significantly more bending. There an eccentricity of the load is present already. ~~This problem is perhaps of theoretical nature. Small displacements are aimed for after all. And its extent may be limited but cannot be ruled out before it has been checked. The structural behaviour of shell structures is not that predictable. Geometric non-linear analysis is required but does come with a larger effort to be made. The model is slightly more work to set up, results are more cumbersome to interpret and the calculations take more time. Within a process of design, it is more convenient to use linear static analysis and check the results in geometric non-linear analysis now and then. Results mentioned in the following text are results from linear static analysis.~~ To exclude significant discrepancies between linear and geometric nonlinear analysis a comparison has been carried out ~~between the linear static and a geometric non-linear analysis undertaken in 10 equal steps,~~ and is shown in Table 2 and Table 4.

**Structural behaviour under self-weight**

The deflections of the shell in the vertical direction due to self-weight (LC1) can be seen in Figure 14. The figure shows the top view of the shell and scaled deflections in x-, y- and z-direction. The contour colours only present the deflection in the z-direction. From this figure it can be seen that the shell deflects downward. At the centre of the shell a deflection of 7.8 mm is present. The largest deflections occur at the middle of the edges. There the downward deflection is 22.9 mm. Remarkably, in the horizontal direction, the edges deflect inward by 7.2 mm.

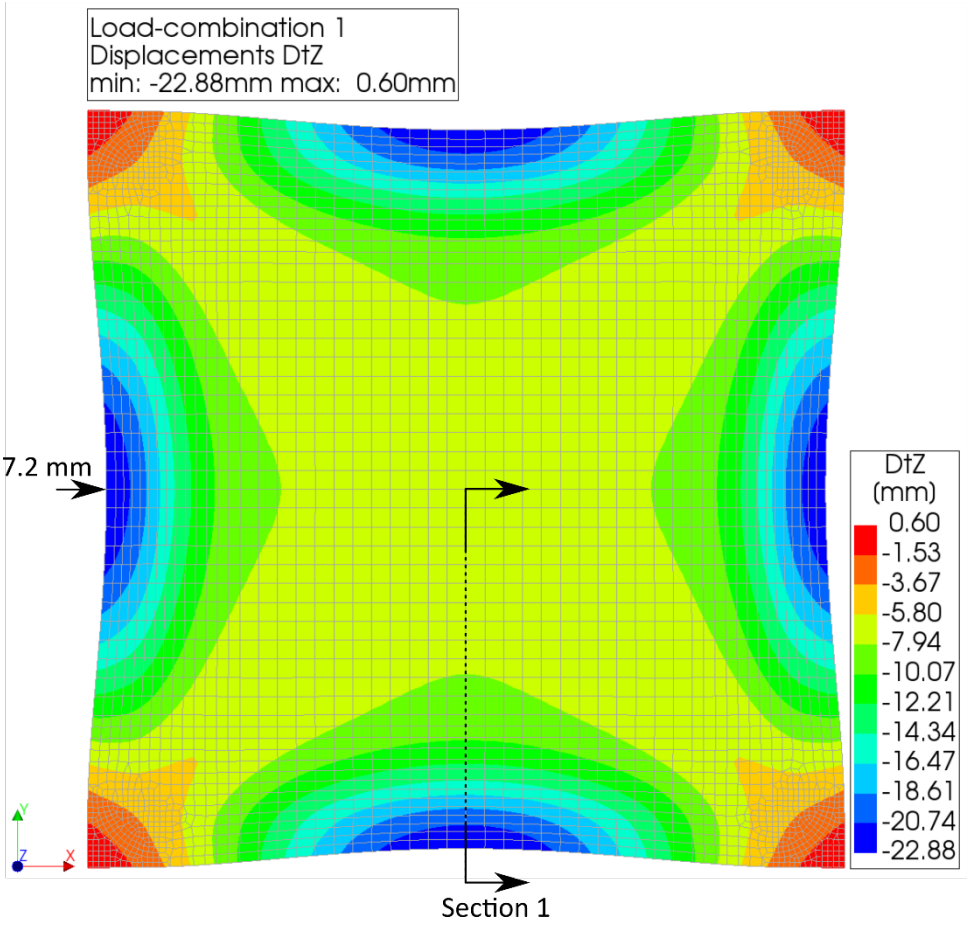


*Figure 14 Top view of deformed shell under self-weight with contour colours for deflection in z-direction*

The latter contradicted the expectation of the authors. Therefore, the results have been compared to the behaviour of a physical model supported at the corners. It should be noted that Isler himself believed in the importance of using physical models to understand the qualitative behaviour of structures, including his own shells. The model was made of a vacuum formed plastic sheet over a CNC milled mould. Its production is out of the scope of this paper. The model could easily and quickly be subjected to various loads applied by hand and can be seen in Figure 15. A vertical applied load showed small but clear inward displacement. In this figure on the right the orange ruler was aligned with the edge before applying the load. The load was applied by a pencil acting as pendulum to ensure loading in vertical direction. In a second setup, the model was laid on the flat surface. Load was applied by hand with spread fingers to represent a distributed vertical load. Then the shell showed clear outward deflection along the edges. Thereby explaining the expectations. These very practical tests have been helpful and convincing that the displayed deflections in the FEA model were indeed correct. Additionally, it has led to an understanding of why this phenomenon occurs which will now be further explained.

*Figure 15 Physical model (left) and manually applied vertical load at the edge (right)*

The edge beam and shell could be considered as a unified cross section. When taking into account a 0.5 m portion of the shell the cross-section is as shown in Figure 16. The principle directions and values of the second moments of area have been determined for this cross-section and are indicated. The values of the first and second principal second moment of area ($I_1$ and $I_2$) have been indicated at scale by the thicker black lines. The second $I_2$ is significantly higher than the first $I_1$. Now considering the load, since the edge is straight there cannot be an in-plane force that brings the vertical load to the supports. The edge is therefore subjected to bending by self-weight. Since the first principal direction $I_1$ is weaker the edge will deform more in this direction and therefore inward.

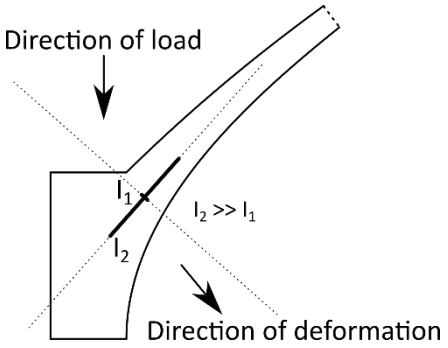


*Figure 16 Cross section of edge and shell showing axes of the principal 2nd moments of area*

Figure 17 shows the principal stresses in the middle layer of the shell in a quarter of the symmetric shell. Since bending stresses in this layer are zero it also represents the principal directions of the normal forces. The largest forces occur in a zone parallel to the edges. In this zone, an arch-like pattern can be observed where the shell is in compression. Thereby the load is transferred to the corners. Along the edges of the shell tensile stresses are present. This can be explained in the following way. In the corner two arches of compression forces coincide pushing the corner outward. Equilibrium of forces must be made within the shell. A slender tensile zone along the edge provides this equilibrium. This can be clearly shown in a simplified strut and tie model as in Figure 18. Also, in Figure 17 along a large portion of the edges only one of the principal directions can be observed since the other is very small. This shows that hardly any load from the shell is transferred towards the beams by in-plane force.

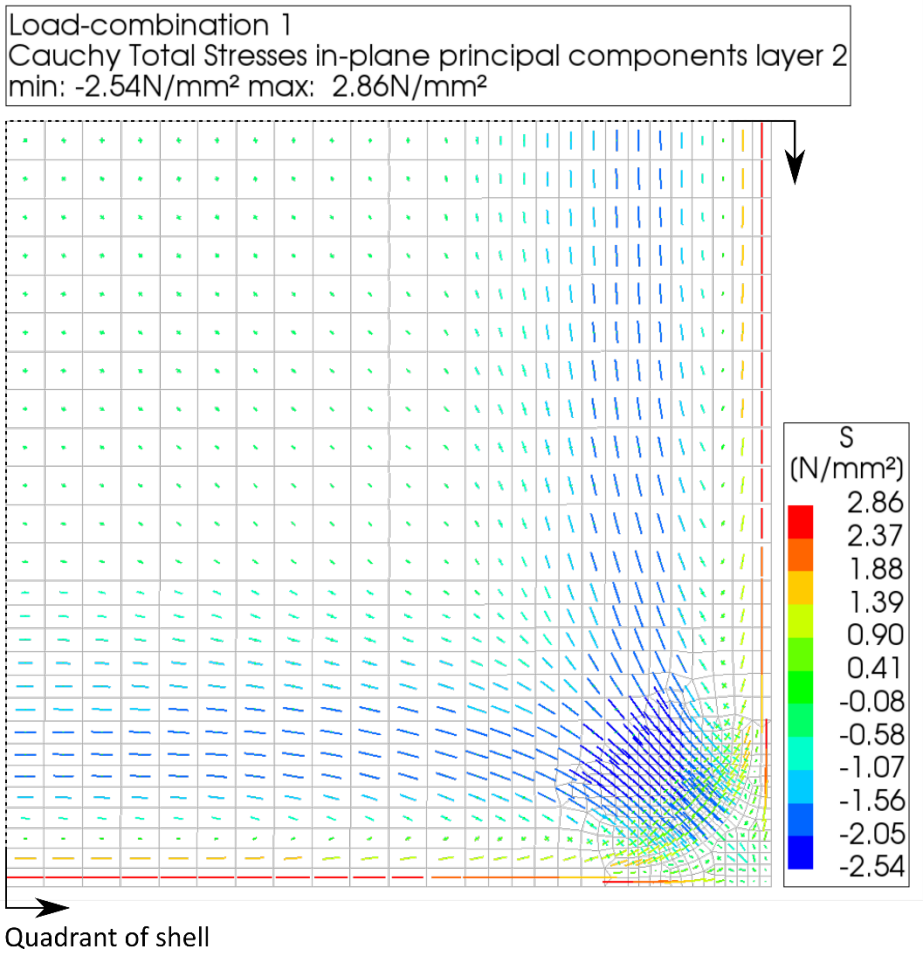

*Figure 17 Principal stresses at the middle layer (layer 2) of the shell for loading by self-weight*

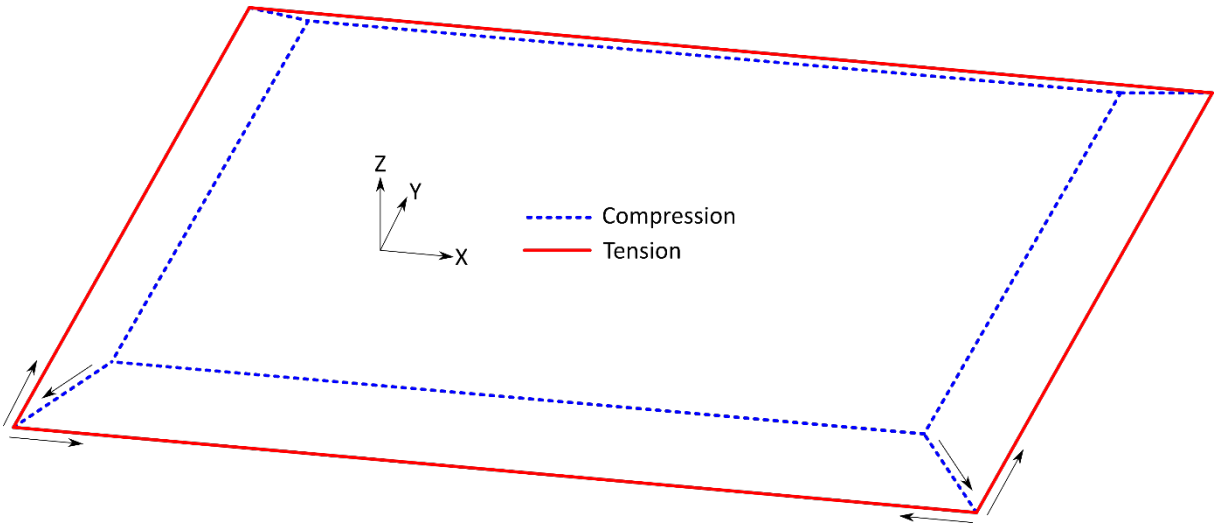


*Figure 18 Strut and tie model for the forces along the edges of the shell*

The stress in the top surface at the centre of the shell is very low. Namely 0.34 N/mm$^2$ in compression. Figure 19 shows the stresses in the x- and y-directions along Section 1 as indicated in Figure 14. Section 1 spans from the edge (distance 0 m) to the centre (distance 10 m) of the shell. Along this section these stresses align with the principal directions. The stresses shown are for the top, middle and bottom surface. Tensile stress occurs in the bottom and top surface. There is bending in the parallel direction of the beam. The sign of the bending moments alternates twice before becoming very small. This supports the above statement about load carried by the edge beam.

In the direction perpendicular to the edge the stresses alternate in sign which shows bending in this direction as well. This is where the direction of the load in the form finding model is different from the actual load by self-weight: namely, perpendicular to the surface versus vertical. Bending can be expected in this area of the shell. Also, these stresses alternate in sign twice and become small at an approximate distance of 6.5 m from the edge. The maximum tensile stress is 2.0 N/mm$^2$. In the middle surface there is hardly any stress, but compression increases towards the centre of the shell.

Lastly, in order to check the above results, the difference with the geometric non-linear analysis is checked. If the difference is low the results of static linear analysis can be assumed to represent the structural behaviour sufficiently. Table 2 shows the comparison for three displacements. The differences are small. The maximum displacement is 22.87 mm which is more than 1/6 of the shell thickness (80 / 6 = 13.3 mm). However, the thickness at that point is actually more than 80 mm and there is hardly any in-plane force along the edge. Further, comparison of stresses in Figure 19, not presented here, showed differences of a similar order to the displacements. The static linear analysis is, therefore, assumed to represent the structural behaviour sufficiently well.

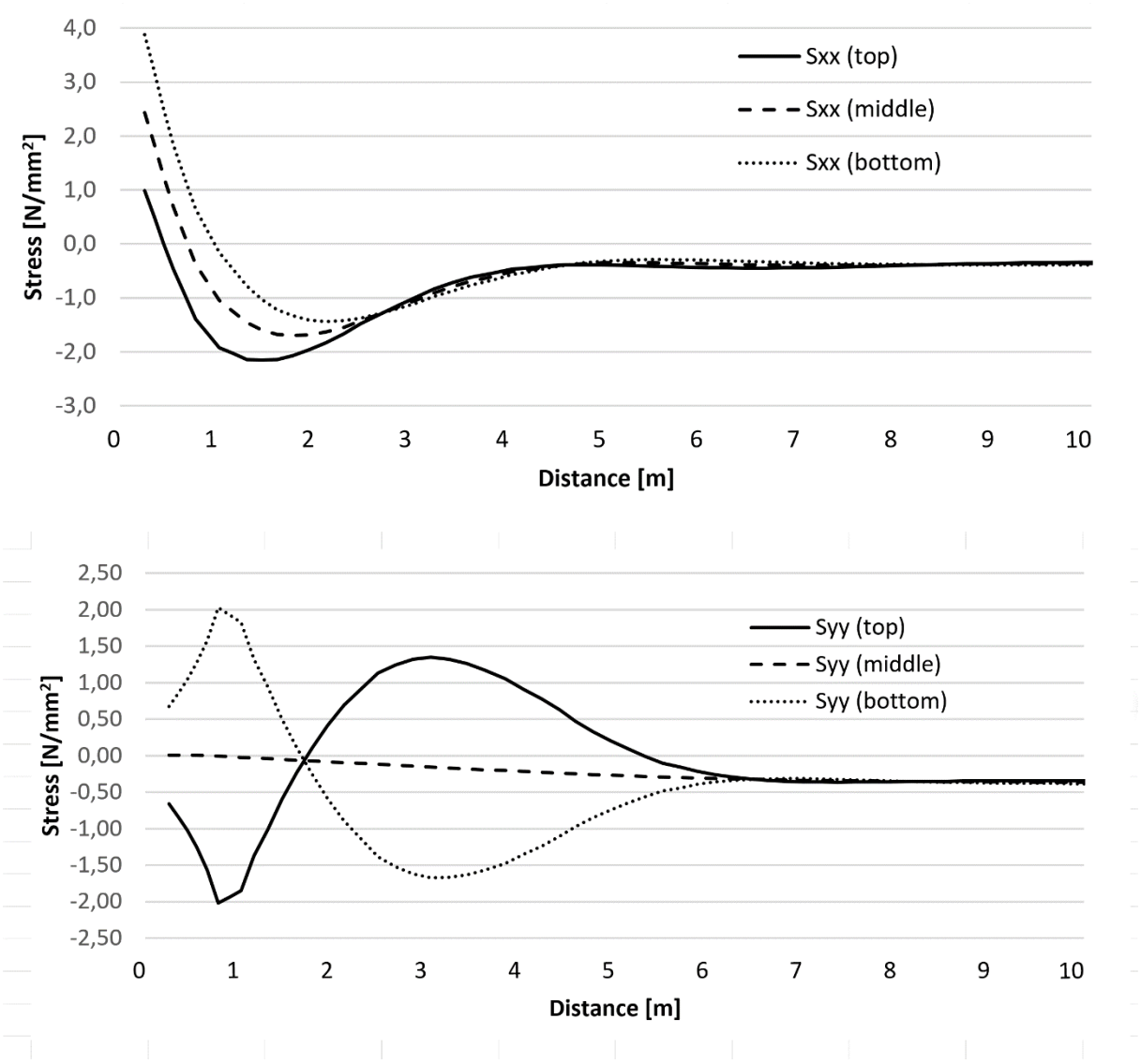


*Figure 19 Stresses along section 1 in x-direction parallel to the edge (top) and y-direction perpendicular to the edge (bottom) for loading by self-weight*

| Description | Unit | Linear static | Geometric non-linear | Difference |
|---|---|---|---|---|
| DtZ centre shell | mm | 7.76 | 7.63 | 0.13 / 1.68% |
| DtZ edge shell | mm | 22.87 | 22.24 | 0.63 / 2.75% |
| DtX edge shell | mm | 7.20 | 6.95 | 0.25 / 3.47% |

*Table 2 Selected results for LC1 (Self-weight)*

To check the overall validity of the FEA model some checks have been performed. Within FEA models the equilibrium of support reactions and applied loads are known to be satisfied locally in a weak sense. Therefore, support reactions may not be exact, but they are always in perfect equilibrium with the load [18]. In Table 3 the following results have been checked using the following analytical calculations: (1) total mass of structure without varying thickness of the shell. (2) The deflection of the edge beam due to its self-weight assuming it is fixed on both ends. This can be done because most of the load is transferred to the corners and not to the beam. (3) The membrane forces at the centre of the shell using the equation for a soap film for a sphere: $\frac{2}{R} = \frac{P}{S}$ [19]. Here, R = 28.99 m which is equal to both principle radii of curvatures measured from the model and P = 1962 N/m$^2$ is the self-weight of the concrete. This can be done since at the centre of the shell it is both symmetric and in pure compression.

The results match reasonably well. The support reaction differs because the variation of thickness has not been taken into account for the analytical calculation. The other differences can be explained by assumptions oversimplifying the structure. However, the membrane force matches very well.

| Description | Unit | Analytical | FEA model | Difference |
|---|---|---|---|---|
| ~~Total vertical s~~Support reactions | N | 1319445 | 0.1417E7 | 97555 / 7.4% |
| Deflection edge beam | mm | 20.2 | 22.9 | 2.7 / 13.4% |
| Membrane force ~~equation for soap film~~ | N/m~~m~~ | 28439 | 29032 | 593 / 2.1% |

*Table 3 Comparison of analytical and FEA results*

**Effect of pre-stress**

The following discussed results combine both self-weight and pre-stress (LC3). The deflections of the shell in the vertical direction can be seen in Figure 20. At the centre of the shell an upward deflection of 11.0 mm is present. The largest deflections occur in the shell approximately 2 m from the edge beam. Here the deflection is 12.2 mm upward. At the edge beam the deflection is 8.6 upward. In the horizontal direction, the deflections at the mid-point of the edges is 1.7 mm inward, although the figure seems to show otherwise. This is because, close to the corners, the edge deforms inwards more. Due to the pre-stress the shell is deflecting upwards instead of downwards. Thereby the shell lifts from the formwork after reaching the full pretension force. The pre-stress prevents the edges from moving inwards. They remain practically in their original position in the horizontal direction.

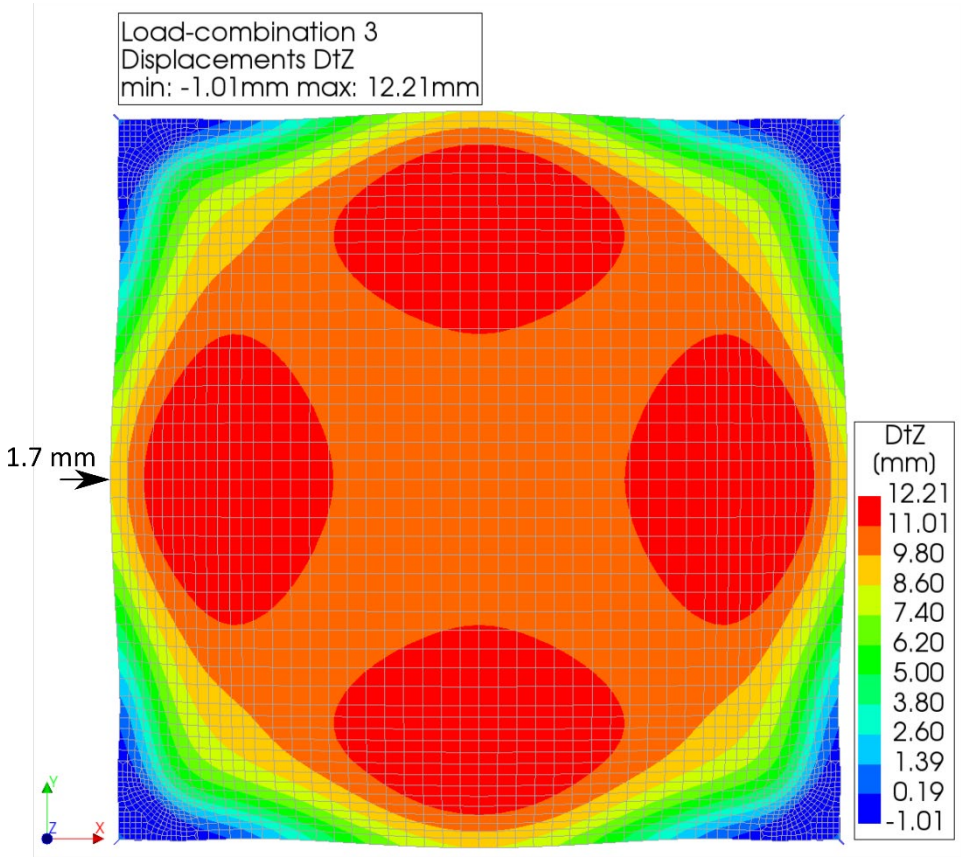


*Figure 20 Top view of deformed shell under self-weight and pretension with contour colours for deflection in z-direction*

Figure 21 shows the principal stresses in the middle layer of the shell. The largest forces now occur in a zone parallel to the edges. In this zone, an arch-like pattern can still be observed, where the shell is

in compression. The tension zone parallel to the edge is no longer present. The entire is edge is now in compression. Also, in this direction the entire middle surface of the shell is in compression.

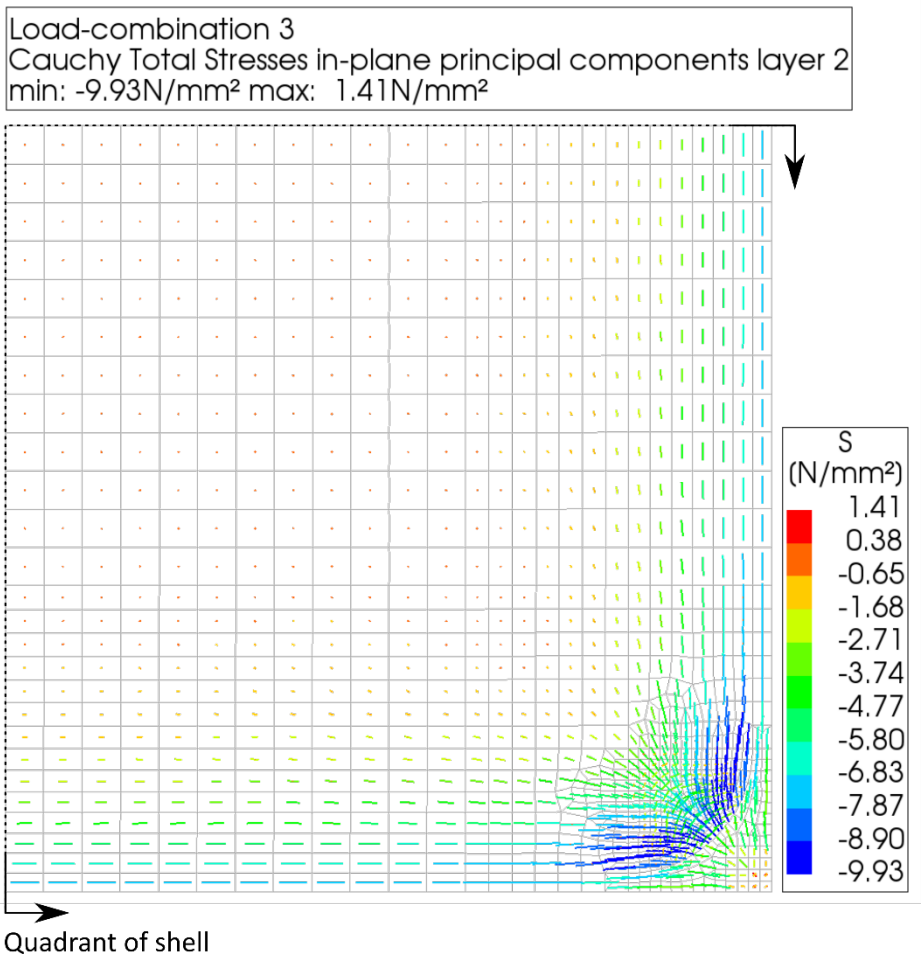


*Figure 21 Principal stresses at the middle layer (layer 2) for combined loading by self-weight and pre-stressing*

The stress in the top surface at the centre of the shell is still very low, but has slightly increased to 0.39 N/mm$^2$ in compression. Figure 22 shows the stresses along Section 1 in both x- and y-directions for the top, middle and bottom layer. The shell surface near the edge no longer has tensile stress in the x-direction parallel to the edge. And the stresses do not alternate in sign. In the perpendicular direction the stress close to the edge is now 1.2 N/mm$^2$ in compression for the bottom surface and 1.2 N/mm$^2$ in tension at the top surface. The bending moment has reversed and is slightly reduced. But the distance from the edge in which bending occurs has increase to approximately 8 m.

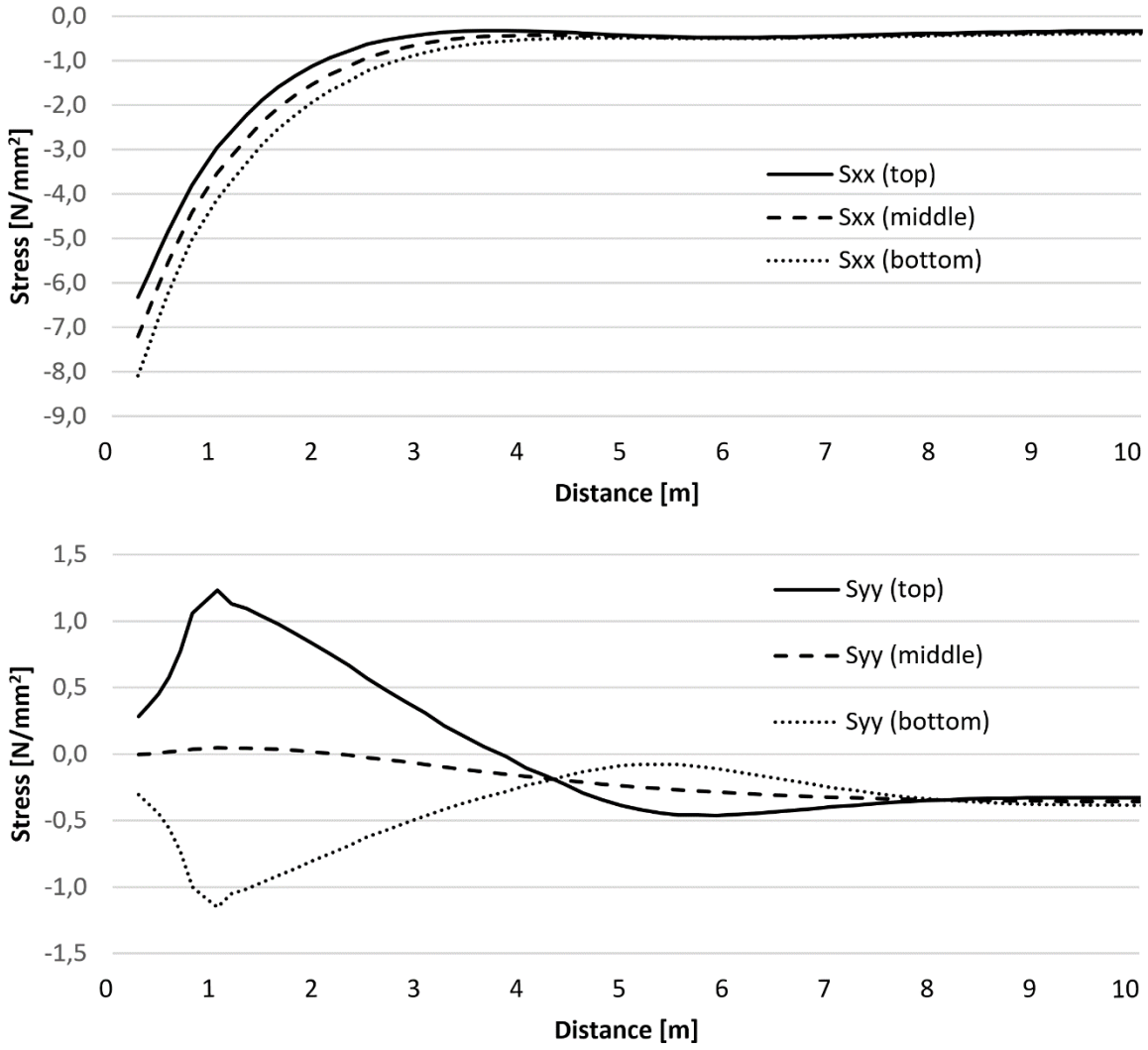


*Figure 22 Stresses along section 1 in x-direction parallel to the edge (top) and y-direction perpendicular (bottom) for loading by self-weight and pre-stress*

The overall effect of the pre-stressing is a reduction of unwanted displacements and stresses. Comparing the displacements with and without pre-stress it shows that the shell is lifted upwards instead of deflecting downwards. The whole surface is pre-cambered by the pre-stress force, which induces even more upward deflection than the downward deflection caused by the self-weight. This could be advantageous for further loading, for example, by snow. By pre-stressing, the edges are prevented from moving inwards. However, additional loading will increase the inward deflection of the edges.

The tensile stresses parallel to the edges are compensated by the pre-stress. Section 1 after pre-stress is fully in compression. However, there are still tensile stresses perpendicular to the edge, although the tensile stresses have been reduced to a maximum of 1.2 N/mm$^2$. The zone closest to the edge still has tensile stress in the top surface of the shell. This is remarkable, since Isler mentioned that the top surface of the shell is in full compression, resulting in a waterproof surface. The found stress could crack the concrete, making it dependent on the quality and strength of the concrete. A general rule of thumb for allowable concrete tensile stress is 10% of its compression strength. Isler mentions in this context “applying the science of modern concrete technology “ in one of his publication on the bubble shells [6], but no specifics are mentioned. Nor how this would help to prevent cracking. The applied

loads do not include snow. From examination of the effect of self-weight load, it can be seen that this would decrease the tensile stress perpendicular to the edge, but increase tensile stress after the sign of the bending moment has changed. This shows that choosing the applied pre-stress force must be a balanced decision for which no one perfect solution exists that satisfies all requirements. Since the tensile stress is relatively low the concrete does not necessarily crack and Isler could still be correct.

But it must be noted that there is a delicate balance between the applied loads and the pre-stress force which must be found by trial and error, and knowing what to look for and where. It is not obvious what the effects of the loading will be. Hence experience is an important factor in shell design.

Considering that Isler determined stresses by measuring strain on a physical model, it could be that this quite local tensile stress would have been difficult to find. There is a limited number of strain gauges that can be placed on a physical model. Also, for different directions more or larger gauges are required. A distance of 3.9 m at 1:50 scale is 78 mm, which is practically a very limited space for multiple gauges. The position of these gauges must have been chosen without knowing the exact position of the largest stresses. Figure 23 is a close up of Figure 2. It is the measuring model of Isler for the rectangular bubble shells. Isler applied strain gauges along the middle section (equivalent to Section 1). The number of wires provides some sense of the number of strain gauges. There are gauges applied to the edge beam and a maximum of two in the area where tension is found in the FEA model. This is not sufficient to obtain the same level of detailed results as a FEA model shows.

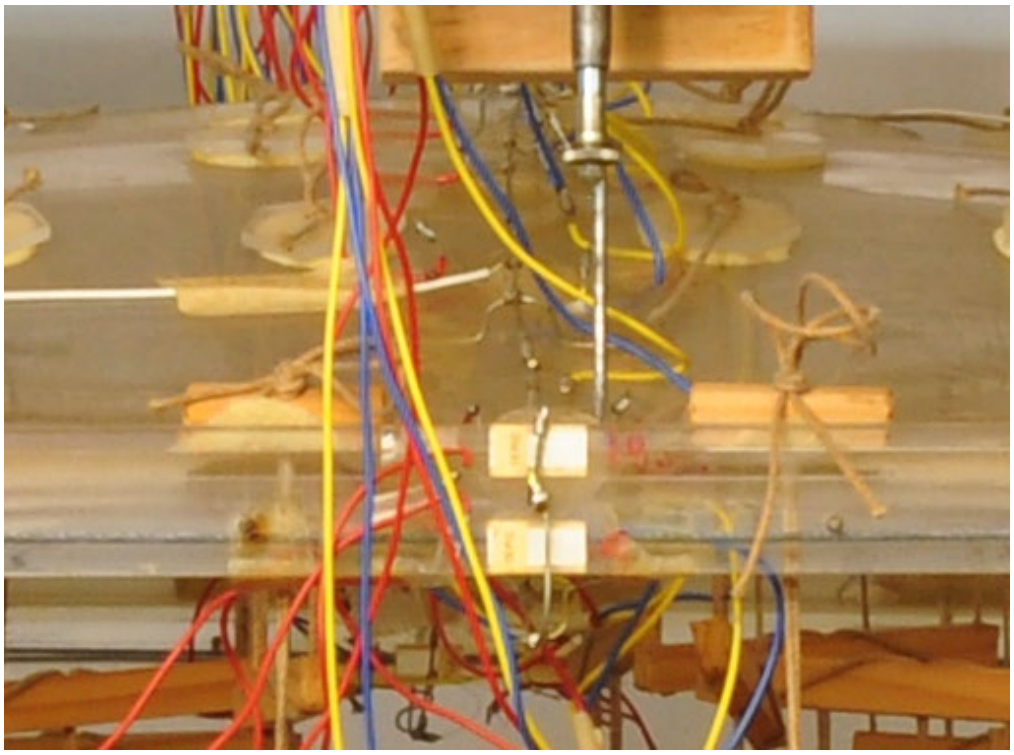

*Figure 23 Close up of measuring model of Isler. Wires give an impression of the number of strain gauges applied. (Photo: © gta Archives / ETH Zurich (Heinz Isler Archive - 217))*

Similar to the first load case, the results of linear elastic analysis for combined self-weight and pre-stress will be compared to the results from the geometrically non-linear analysis. The comparison can be seen in Table 4. For displacement, a significant difference is found at the edges of the shell. Therefore, the stresses are compared as well and found to be higher after non-linear analysis. For stress analysis the difference can be of importance since the stress is close to the maximum tensile

capacity of concrete. The general trend of stress distribution is practically equal to that of the static linear analysis.

| Description | Unit | Linear static | Geometric non-linear | Difference |
|---|---|---|---|---|
| DtZ centre shell | mm | 11.01 | 11.16 | 0.15 / 1.36 |
| DtZ edge shell | mm | 8.63 | 10.11 | 1.48 / 17.15% |
| DtX edge shell | mm | 1.73 | 1.05 | 0.68 / 39.31% |
| Sxx edge shell (bottom) | $N/mm^2$ | -10.07 | -10.48 | 0.41 / 4.07% |

*Table 4 Selected results for LC3 (Self weight + pre-stress)*

**Membrane behaviour**

Isler points out that a good shell is one that shows little displacement over the course of its lifetime. This is described in [20]. As a reference Isler uses a ratio of deflection to span of the shell. According to Isler, the largest built bubble shell has a deflection to span ratio of approximately 1/3300. Using the above result for deflection under self-weight the following ratios can be found:

7.8 / 20000 ≈ 1 / 2564 at the centre of the shell

22.8 / 20000 ≈ 1 / 877 at the middle of the shell edge

Membrane behaviour can also be evaluated by the contribution of membrane action to the total stress and expressed as a ratio, or, simultaneously, the contribution of bending action to the total stress. This is shown in Figure 24. Calculations to do so have been described by A. Borgart (dissertation expected mid 2020) and have been applied by Q. Li [21] In this manner the stresses throughout the entire cross section are assessed in one factor instead of considering top, middle and bottom layer separately. In this figure the horizontal axis represents the contribution of membrane action to the total stress. These can be both positive and negative. The vertical axis represents the same for bending action. For example, when no bending is present the shell becomes a membrane. A point will lie on the horizontal axis. A membrane under compression is here considered ideal for a shell. In a different case, when there is only bending, a point lies on the vertical axis.

These ratios can be found for various directions. For example, the principal directions of the membrane forces or the bending moment. These do not necessary align. Here the ratios have been determined for the two principal directions of the membrane forces. Based on Nxx, Nyy and Nxy the principal directions $\alpha_0$ and $\alpha_0 + \pi/2$ can be found. $R_1$ denotes the ratio in the direction of the first principal membrane force, and $R_2$ denotes that in the direction of the second principal ~~normal~~ membrane force. A ratio can be found for each element of the FEA model. Also, the area of each mesh element can be found. These have been used to create histograms which describe the area for which the ratio is within an indicated range. The ratios will now be assessed for the bubble shell.

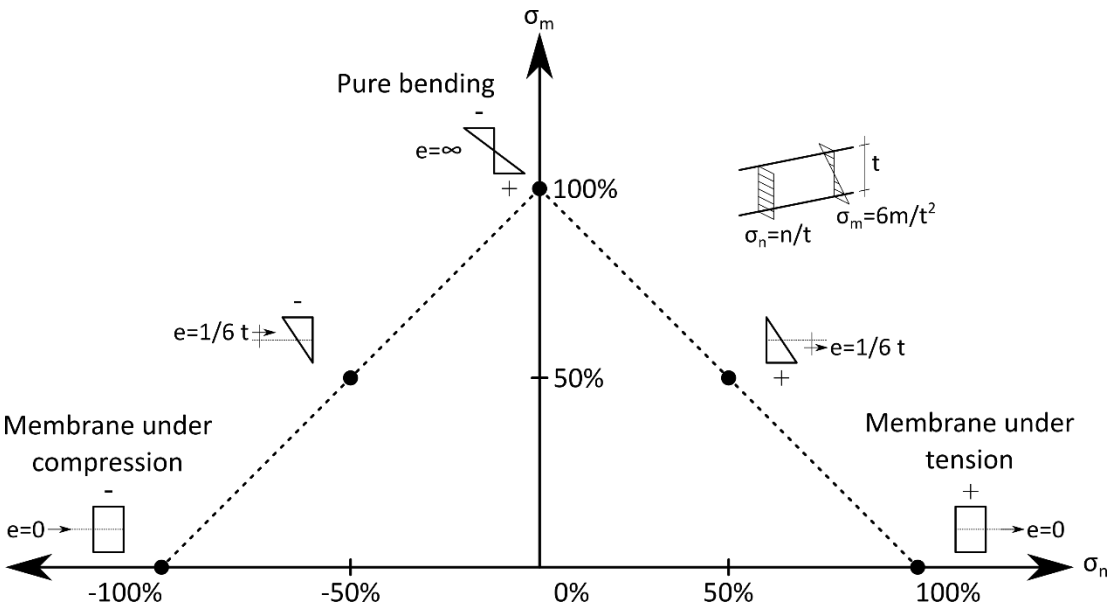


*Figure 24 Ratio graph for stress due to normal force and bending (Modified from: A. Borgart)*

Figure 25 and **Error! Reference source not found.** show contour plots and histograms of the results. First for self-weight only (LC1) and second for self-weight and pre-stress (LC3). The ratios R1 and R2 are shown for the principal directions of the membrane force N1 and N2 which are the directions as can be seen in Figure 17. The same results are presented in a different manner below. Here the ratios are presented in histograms as percentage of the shell area. This way, for example, the proportion of the shell area that is fully in compression can be assessed. This was found by taking into account the stress at the centre of each mesh element and its area.

The principal forces can be both negative, positive or be a combination. Typically, the larger compression force is N2. For this shell the ratios show, largely, a surface in compression when looking at N2. As shown for R2, due to self-weight (LC1) (27+30+13+11+4=) 85% of the shell area is in compression only for this direction. A total (2+3+1+2+6+1=) 15% is a combination of tension and compression. Of the latter, 1% of the results have tension in the middle surface. The overall impression of these results can be defined as good membrane behaviour. However, for the first principal force direction, R1, only (14+2+3+1+3=) 23% of the shell area is fully compressed, (4+3+6+27+17+20=) 67% of the shell is a combination of tension and compression of which 20% of the result have tension in the middle surface.

Now looking at the combination of self-weight and pre-stress (LC3), for N2, 99% of the shell area is in compression only for this direction. Just 1% is a combination of tension and compression. For the first principal force direction N1, only (8+5+3+9+6=) 31% of the shell area is fully compressed, 69% of the shell is a combination of tension and compression of which 20% of the shell area has tension in the middle surface. None of the shell area is in tension only. Compared to loading by self-weight only this is an improvement.

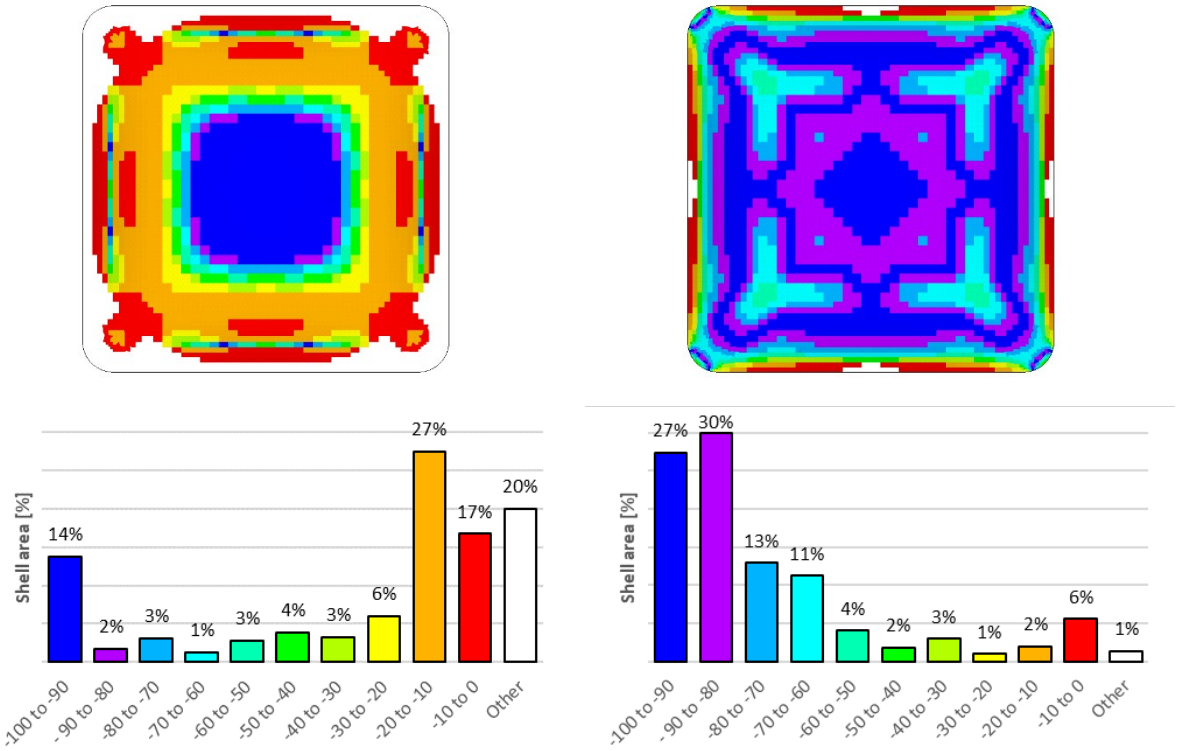


*Figure 25 Stress area ratios R1 (left) and R2 (right) for LC1 in ten steps for negative values*

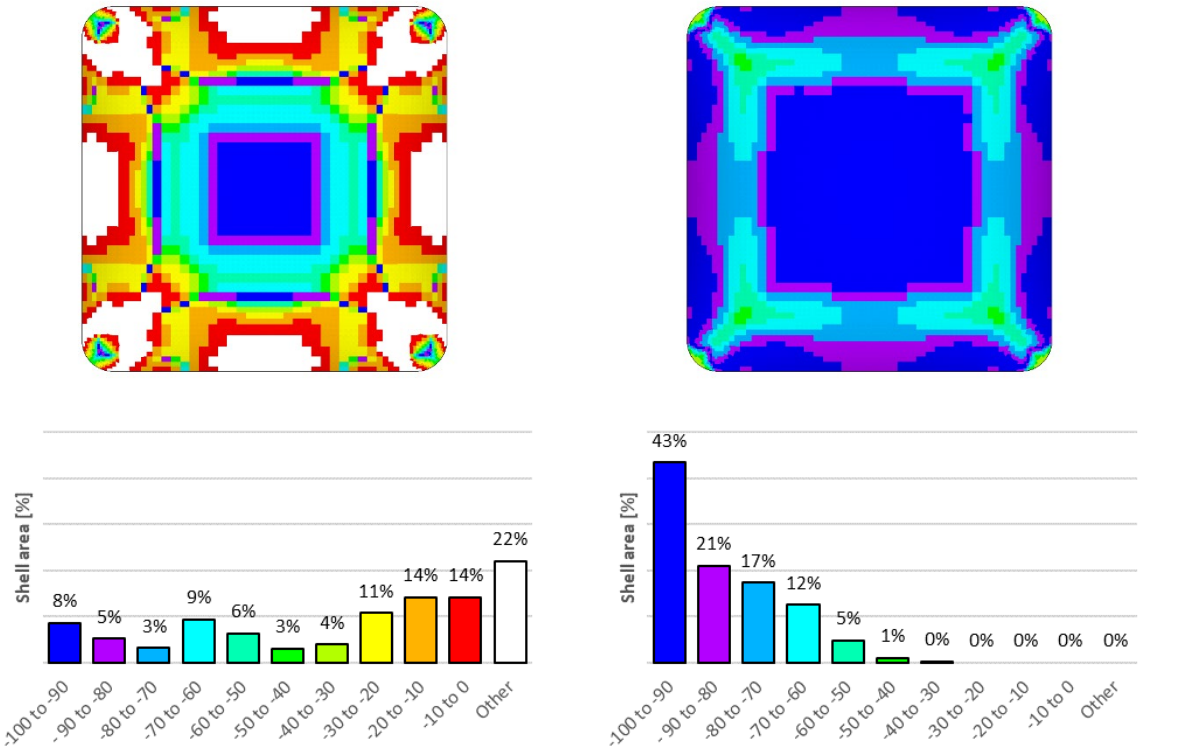


*Figure 26 Stress area ratios R1 (left) and R2 (right) for LC3 in ten steps for negative values*

**Conclusions**

Heinz Isler aimed for small displacements in his shell structures. The presented FEA model indeed showed small displacements when applying both self-weight and pre-stress in the edge beams. The largest deflections found are 22.9 mm downward due to self-weight and 12.2 mm upward after including pre-stress forces. Both occur at the midpoint of the edge beams. The deflection to span ratio, for the shell subjected to self-weight, is close to 1/2564.

Along the edges of the shell structure bending occurs. Both with and without pre-stressing the edges. This results in tensile stresses. The shell structure is not a compression only structure.

The effect of pre-stress has been studied by comparing the structural behaviour of the bubble shell by first excluding pre-stress and second including pre-stress. The pre-stress, as Isler applied it, effectively fulfils three functions: (1) it creates equilibrium of forces at the corners - not applying pre-stress requires internal equilibrium resulting in a tensile zone along the shell edge; (2) the shell is lifted entirely and mostly close to the edges, such that it would separate from its formwork; (3) parallel to the edge tensile stresses are prevented by pre-stressing. The edge is entirely in compression for this direction. Perpendicular to the edge the alternating bending moment due to self-weight is reduced and reversed by pre-stressing. Most tensile stresses are prevented, but not all. The top surface is mostly in compression after including pre-stress. It includes some reserve for additional loading, like snow. However, there are still low tensile stresses in the shell at the top surface close to the edge beams.

The membrane behaviour has been assessed in both directions of the principal membrane forces. When not taking into account pre-stress, the second principal direction is generally the main load bearing direction where loads are transferred in compression. In this direction bending stresses are not exceeding stresses due to normal forces. Membrane forces are dominant. In the first principal direction, the bending stresses mostly exceed the stresses due to membrane forces. Finding form though inflating a membrane is not sufficient to create a compression only structure and the applied pre-stress forces cannot completely compensate for all tensile stresses. Pre-stress is required to prevent most of the tensile stress. The membrane behaviour improves significantly by adding the pre-stress.

Shell assessment ratios for membrane behaviour provide insight into the structural behaviour of the shell. Shell behaviour must be assessed in multiple~~both principal~~ directions. For the presented shell, in the first principal direction of the normal force the shell exhibits an area with low membrane behaviour although the shell is thought to be compression only which is it not.

**Discussion**

Within the design of shell structures emphasis is often on finding the shape of the structure. Less attention is given to the processes that follows, to construction and even beyond. Reverse engineering of the presented shell structures shows that the entire process is a series of steps of which finding a shape is the first. Each step responds to the previous and each is equally important. Isler must have carefully developed and studied unconventional solutions until satisfactory results were obtained. One of those is the application of pre-stress which is the subject of this study. This study shows how Isler used pre-stress to influence and improve the structural behaviour of the bubble shells.

In a broad perspective of shell design, the engineer must be skilled to find solutions for any state of stress. A shell structure might be close to a compression only structure, but more load cases must be considered from which tensile stresses will occur. Perhaps the main challenge of designing shell

structures is not to find a shape, but merely to solve or control the unwanted aspects of its structural behaviour in its specific context. Something for which Isler obviously developed exceptional skills. The question is not how to create a compression only structure, but how to make, the structure as a whole, function under all relevant load cases, something that inevitably results in compromises.

Structural analysis can often be simplified. When the aspects; loads, geometry, boundary conditions and material properties are limited in their complexity laws of mechanics clearly describe the structural behaviour. In that case, internal forces, displacements and stresses can be determined. Within thin shell structures all the aspects are complex. Simplifications cannot be made easily. The analysis must be done by a knowledgeable person in the field of mechanics with an eye for the unexpected and a considerable amount of patience.

Lastly, Isler mentions that the main load of the shell is transferred to the corners [5]. He specifies 22.5% of the shells self-weight is transferred to the corners in the case where the shell is supported by walls. The results in this paper confirm load transfer to the corners. However, the used boundary conditions are not equal to the case described by Isler. The authors have modelled th~~is~~e case~~situation~~, by applying the boundary conditions directly on the shell edge. Vertical translation has thereby been constrained. This has been found to result in ~~and have found~~ concentrated shear forces in the corners. These are known from classic theory of plates and apply to plane stress situations. In the physical models of Isler, the practical implementation of constraining ~~Depending on how Isler would constrain~~ the edges would have determined whether these concentrated shear forces ~~would~~ occur ~~or not~~. Namely, have means been applied to restrict downward support reactions or would the edge be free to move upward? This raises the question: how did Isler come to the above ~~this~~ conclusion? Additionally, knowing the support reactions are distributed a certain distance from the corner must be taken into account. So, what can be considered “the corner”? More models should be made in an attempt to answer that question. Different types of models are required. Physical models to determine how Isler could have measured or derived a distributed support reaction. And computational non-linear FEA models which include contact elements that simulate a support condition providing support in an upward direction but not in a downward direction. Default linear static analysis, as already modelled, provides support in both directions. The authors intend to study this further.

**Acknowledgements**

The authors would like to thank Rainer Schützeichel and Giulia Boller of the ETH Zürich for their support for visiting the archive of Isler’s legacy and for the many discussions on the work of Isler. Similar thanks for discussions, feedback and support by Roel Schipper of the TU Delft. Also, thanks to the people of the gta Archive in Zürich for their work on archiving the endless volume of documents and support during the visit to the archive. Lastly, the authors express their appreciation for the CIMIS (Candela-Isler-Müther International Symposium) for creating a community that exchanges and promotes essential historical information that various archives contain.

**References**

[1] H. Isler, "Personal correspondence to Prof. D.P. Billington, 2002," in *gta Archive, Eidgenössische Technische Hochschule, Estate of Heinz Isler*. Zurich.

[2] H. Isler, "Personal correspondence to Prof. F. Frey, 1993," in *gta Archive, Eidgenössische Technische Hochschule, Estate of Heinz Isler (Swimming pool Heimberg 217-0370)*. Zurich.

[3] P. Eigenraam and A. Borgart, "Reverse engineering of free form shell structures; From point cloud to finite element model," *Heron,* vol. 61, no. 3, pp. 193-210, 2016. [Online]. Available: http://heronjournal.nl/61-3/5.pdf.

[4] E. Ramm and E. Schunck, *Heinz Isler, Schalen: Katalog zur Ausstellung*. vdf, Hochsch.-Verlag an der ETH, 1986.
[5] J. Chilton, *Heinz Isler, The Engineer's Contribution to Contemporary Architecture*. Thomas Telford, 2000.
[6] H. Isler, "Doce anos de aplicacion de cascarones tipo burbuja," presented at the Instituto Mexicano del Cemento Y del Concrete and the International Association for Shell Structures, Mexico, 1968.
[7] H. Isler, "Measuring model for Bubble shells," in *gta Archive, Eidgenössische Technische Hochschule, Estate of Heinz Isler*. Zurich.
[8] Rhinoceros. https://www.rhino3d.com/ (accessed 2019).
[9] Grasshopper. https://www.grasshopper3d.com/ (accessed 2019).
[10] R. Rodricks and A. Heumann. "Online reference for Grasshopper Components: Surface from points." GitHub. (accessed 2019).
[11] H. Isler, "Kabelplan (Doppelschalen)," in *gta Archive, Eidgenössische Technische Hochschule, Estate of Heinz Isler*. Zurich.
[12] "Diana FEA." https://dianafea.com/ (accessed 2019).
[13] "Element Library," in *Diana 10.2 documentation* Delft: Diana FEA BV, 2017.
[14] H. Isler, "Hand calculation / Ablenkungskraft," in *GTA Archive, Eidgenössische Technische Hochschule, Estate of Heinz Isler (Bubble shell Ramseier & Jenzen 217-02)*. Zurich.
[15] C. W. Dolan and H. R. Hamilton, *Prestressed concrete : building, design, and construction*, Cham, Switzerland: Springer, 2019. [Online]. Available: https://doi.org/10.1007/978-3-319-97882-6.
[16] O. C. Zienkiewicz, R. L. Taylor, and J. Z. Zhu, *The Finite Element Method: Its Basis and Fundamentals, Sixth Edition*. Butterworth-Heinemann, 2005.
[17] A. W. M. Kok, *PAO cursus, Eindige-Elementenmethode: schijven, platen en schalen, Course notes Finite Elements*. Delft University of Technology, 2007.
[18] J. Blauwendraad, *Plates and FEM* (Solid Mechanics and Its Applications). Springer Netherlands, 2010.
[19] A. M. Haas, *Design of thin concrete shells Vol. 2, Negative curvature index*. New York: Wiley (in English), 1967.
[20] H. Isler, "New Shapes for Shells - Twenty Years Later," in *Heinz Isler as Structural Artist*, Princeton, New Jersey, 1980: Princeton University Press.
[21] Q. Li, "Form Follows Force," Doctor of Philosophy, Delft University of Technology, 2018.